Generative Network Model Reveals Different Trajectories in Brain Networks of PSA and Stroke Patients

Kangli Dong, *Member, IEEE*, Yuming Zhong, Lu Zhang, Wei Liang, Yue Zhao, Jun Liu, Siya Chen, Seedahmed S. Mahmoud, *Senior Member, IEEE*, and Yu Sun, *Senior Member, IEEE*

***Abstract*— Post-stroke aphasia (PSA), induced by acute brain injury, is an acquired language disorder resulting from stroke, primarily characterized by impairments across multiple linguistic functions including spontaneous speech, auditory comprehension, repetition, naming, reading, and writing. Previous studies have demonstrated that the topological features of healthy brains align with complex networks, whereas key topological features in PSA patients (e.g., interhemispheric connectivity, functional connectivity (FC) of language networks) undergo significant alterations due to acute brain injury. However, traditional graph-theoretical approaches fail to elucidate the dynamic evolutionary patterns underlying functional reorganization in brain networks. Moreover, existing research lacks systematic exploration of trajectory characteristics and economic cost regulation mechanisms in network generation among PSA patients. To address these gaps, this study introduces a framework based on generative network modeling, integrating non-geometric rules (power-law functions of topological relationships) and geometric rules (connection distance calculations) to simulate the formation process of functional brain networks. By parametrically modulating the balance between nodal connection propensity and distance cost, and comparing the optimal matching between simulated and observed networks, we explored the evolutionary mechanism of brain networks in PSA patients. Key findings include: For the FC matrix with 10% sparsity, 1) The homogeneous model combined with geometric distance-based economic costs generates optimal simulated networks; 2) PSA patients exhibit significantly higher absolute values of parameter η compared to general stroke patients ($p < 0.05$), indicating increased economic costs for connections with distal nodes; 3) PSA patients show the highest γ values, with significant reduction in inter-nodal connection propensity versus healthy controls ($p < 0.05$), suggesting impaired network integration efficiency; 4) Trajectory analysis reveals decreased parametric values in thalamus-related regions but elevated values in occipital and cerebellar regions among PSA patients, with distance costs showing negative correlation with stroke patients ($R^2 = 0.86$), uncovering region-specific trajectories of functional reorganization around lesions. By constructing a computational model incorporating economic clustering rules, this study clarifies differential network evolution patterns between PSA and general stroke patients, provides theoretical foundations for targeted neuromodulation and intervention strategy optimization, and addresses the limitations of traditional graph theory in dynamic mechanism analysis.**

***Index Terms*— Post-stroke aphasia, generative network, functional connectivity, graph theory.**

Received 12 October 2024; revised 22 May 2025 and 15 June 2025; accepted 16 July 2025. Date of publication 21 July 2025; date of current version 31 July 2025. This work was supported in part by Guangdong Basic and Applied Basic Research Foundation, China, under Grant 2025A1515012149 and Grant 2025A1515010808; in part by the 2020 Li Ka Shing Foundation Cross-Disciplinary Research Grant under Grant 2020LKSFG04C; in part by the National Natural Science Foundation of China under Grant 82172056; in part by Zhejiang Provincial Natural Science Foundation of China under Grant LR23F010003; in part by the National Key Research and Development Program of China under Grant 2022ZD0117902; and in part by the Shantou University (STU) Scientific Research Initiation, China, under Grant NTF24004T. *(Kangli Dong and Yuming Zhong contributed equally to this work.) (Corresponding authors: Siya Chen; Seedahmed S. Mahmoud.)*

This work involved human subjects or animals in its research. Approval of all ethical and experimental procedures and protocols was granted in part by the IRB at the University of South Carolina under Application No. Pro00132576 and in part by the University of North Carolina at Greensboro (UNCG) Institutional Review Board.

Kangli Dong and Seedahmed S. Mahmoud are with the Department of Biomedical Engineering, College of Engineering, Shantou University, Shantou, Guangdong 515063, China (e-mail: mahmoud@stu.edu.cn).

Yuming Zhong is with the Department of Imaging and Interventional Radiology, The Chinese University of Hong Kong, Hong Kong, SAR, China, and also with the Department of Biomedical Engineering, College of Engineering, Shantou University, Shantou, Guangdong 515063, China.

Lu Zhang is with the Department of Rehabilitation, Sir Run Run Shaw Hospital, Zhejiang University School of Medicine, Zhejiang University, Hangzhou, Zhejiang 310027, China.

Wei Liang is with the Department of Computer Science and Engineering, Lehigh University, Bethlehem, PA 18015 USA.

Yue Zhao is with the Department of Urology, Xiang'an Hospital, Xiamen University, Xiamen, Fujian 361102, China.

Jun Liu and Yu Sun are with the Key Laboratory for Biomedical Engineering of Ministry of Education of China, Zhejiang University, Hangzhou 310027, China.

Siya Chen is with the School of Computer Science and Technology, Dongguan University of Technology, Dongguan, Guangdong 523808, China (e-mail: sychen0622@gmail.com).

This article has supplementary downloadable material available at https://doi.org/10.1109/TNSRE.2025.3590826, provided by the authors.

Digital Object Identifier 10.1109/TNSRE.2025.3590826

I. Introduction

STROKE is a brain disease that arises from multiple factors damaging the blood vessels of the brain, leading to localized or widespread damage to brain organization, which continued to rank as the second-highest Level 3 cause of mortality and the third-highest Level 3 cause of both death and disability globally in 2019 [1]. Stroke is a significant cause of aphasia, leading to the loss of language function in patients dueto acute brain injury [2], [3]. The long and short-term loss of speech function and the complex transformations

of different types of post-stroke aphasia (PSA) during the recovery period make the rehabilitation of aphasia particularly challenging [4].

As the primary target of stroke, the brain acts as a vast and complex network, where different brain atlases divide the brain into various regions based on anatomy or brain function. The functional connections between regions are considered as nodes and edges of a graph, forming a brain functional connectivity (FC) matrix that represents the network of connections between brain regions. Due to the availability of large public datasets and freely accessible highly integrated toolboxes [5], [6], [7], the application of graph theory principles on network neuroscience has become widespread [8], [9], [10], [11], [12], [13], [14], [15], [16]. Representing the connections between neurons and neural elements in the brain as a graph, analyzing network topology and characteristics has been a common approach to explore the complexity of the brain. Graph theory analysis reveals several key properties of healthy brain networks, including small-world characteristics with short and efficient connections between nodes [17], [18], highly central hubs with a power-law distribution of node degrees [19], [20], modular organization of different brain regions based on functional modules or network subsystems [21], [22], and rich club structures formed by densely connected hub nodes [23]. Many studies have demonstrated that aphasia can alter the topological structure and graph theory properties of the brain, providing insights into the mechanism behind primary aphasia [14], [15] and the aphasia caused by stroke [16], [24]. Chen et al. [16] compared whole-brain FC networks constructed using Power264 atlas in 24 right-handed PSA patients and 19 healthy controls, and found that small-worldness, normalised clustering coefficients, and local efficiency values were reduced and that local efficiency values were positively correlated with linguistic competence, repetition, naming, and auditory comprehension in PSA patients. Johnson et al. [24] explored changes in graph theoretic properties in 26 PSA patients before and after speech therapy and revealed that patients' mean network strength and overall efficiency controlled lesion volume and predicted treatment outcome. The graph theory-based statistics provide a concise description of the organisational features of brain networks, including the functional balancing that supports the segregation and integration of brain functions [25] while emphasizing the trade-off between cost and function [26].

Although graph theory-based statistics are useful for finding disease biomarkers by comparing healthy individuals and patients, they provide limited insight into the mechanisms of network function, growth, and evolution [27]. Aphasia typically involves long-term or short-term periods of illness and recovery processes that are accompanied by the destruction and recovery of FCs of brain networks over time, under the support of plasticity [28], [29]. These processes are beyond the insights that can be provided by existing commonly used graph-theoretical statistics. To shift the focus from graph-theoretical statistics to mechanisms and processes, the network generative model is a flexible framework for generating synthetic networks from a set of parameterized wiring rules [30], [31]. As long as the wiring rules are sufficiently informed and have a biological basis, generative models can be used to test and identify potential mechanisms of growth and evolution of biological neural networks. With these mechanisms, it is possible to distinguish topological features that drive network growth from those that appear only as byproducts [32], and to take targeted intervention measures [33]. This study aims to investigate the growth and evolution of brain networks under PSA by constructing network generative models, and further provide potential interventions for PSA rehabilitation. Specifically, we utilized a dual-parameter model, incorporating connections formed based on non-geometric rules on a shared topological relationship and a power-law function based on the geometric rules of interregional connectivity distances in the brain [34], [35]. Over time, a simulated brain network was probabilistically formed to analyze the overall model performance and compare the differences between the simulated network and the real network directly. To generate more accurate simulated networks, we used a traversal method to adjust model parameters, revealing finer rules of network wiring. These simulated networks exhibited similar characteristics to observed real networks, further elucidating the differences and underlying mechanisms of different types of PSA.

The following sections of the article will be presented in the following order: Section II presents the research methodology, including an introduction to the datasets, data preprocessing procedures, and the formation of brain networks based on wiring rules in probability order over time, followed by an introduction to statistical analysis methods for comparing the differences between generated networks and observed networks. Section III focuses on the mathematical model construction of the generative simulation network and the results of the statistical analysis with the observed network. Section IV discusses the results and drawbacks of simulating generative networks. Section V summarizes the overall work.

II. Methods

A. Datasets

1) Participants and fMRI Acquisition: In order to achieve the goal of investigating the differences between the growth of PSA brain networks and observed networks by constructing a generative model of functional brain networks, we integrated two publicly available datasets for analysis, which are described below:

Dataset 1: Resting-state fMRI scans were acquired from the University of South Carolina and the Medical University of South Carolina [36]. The Institutional Review Board (IRB) at the University of South Carolina determined that the study was exempt from further review. The dataset included 148 PSA patients and 26 general stroke patients after excluding patients with head motion exceeding 3mm. For each patient, the fMRI scan closest to the stroke onset time was selected. Participants were instructed to remain still in the scanner with their eyes open and stay awake. All fMRI images were acquired using a Siemens Trio 3.0T scanner equipped with a 16-channel head coil.

Dataset 2: 28 healthy participants served as a control group and underwent whole-brain imaging at UNCG's Gateway MRI

Center using a Siemens 3.0T Tim Trio MRI scanner with a 16-channel head coil. The study was approved by the University of North Carolina at Greensboro IRB [37]. Resting-state functional data were collected after the anatomical scans, and 300 measurements were taken during the 10-minute scans. Subjects were asked to remain quiet and awake with their eyes open. Functional scans were acquired using echo-planar image sequences sensitive to blood oxygen level-dependent (BOLD) contrast, with a scan thickness of 4.0 mm, 32 slices, a TE of 30 ms, a TR of 2000 ms, and a flip angle of 70. The scans sequentially covered the entire cerebral cortex and part of the cerebellum.

The initial aim of this dataset was to investigate the ability of connectome-based modeling approaches exploring intrinsic FC in default mode networks to predict memory discrimination in young versus old adults. In this study, we used this dataset in conjunction with an open-access fMRI dataset with the aim of modelling brain FC in patients with PSA, general stroke patients, and healthy individuals to simulate the generation of brain FC matrices and to explore the modelling of the mechanisms underlying the emergence of PSA. Informed Consent was obtained for both datasets.

2) fMRI Pre-Processing: Before constructing the functional brain network, for the fMRI raw scan data of a total of 202 subjects in the above two datasets, we performed pre-processing operations. The first ten volumes of each scan were excluded to ensure magnetic stability and to optimize the generation of a consistent blood oxygenation level-dependent (BOLD) activity signal. The preprocessing pipeline was implemented utilizing the Gretna toolbox [7]. Subsequently, the fMRI data underwent the following procedures:

1. Correction for slice timing; 2. Realignment to correct for head motion; 3. Normalization to a 3 mm MNI space using an EPI template provided by the Gretna software package; 4. Application of linear temporal detrending to remove the linear drift of the BOLD signal; 5. Covariate regression, including the white matter signal, cerebrospinal fluid (CSF) signal, and head motion signal, utilising the Fristion-24 Parameters strategy; 6. Temporal filtering with a bandwidth of 0.01-0.1 Hz.

B. Construction of the FC Matrix

The Fair34 brain atlas [38] was used to partition the brain into 34 anatomically meaningful regions, and the averaged BOLD signals of these brain regions were constructed. Pearson correlation calculations were performed on BOLD signals of each brain region to determine the FC strength between different brain regions, resulting in a symmetric brain FC matrix.

The FC matrix for each participant was thresholded to construct a binary network. In order to ensure sparsity, the binary FC matrices were created by preserving more connection information and capturing the relationships between different nodes. We used 5%, 10%, and 15% sparsity thresholds in the initial FC matrices to avoid the subjectivity of threshold selection and better reflect the topological structure of the brain network.

C. Generative Network Models

Based on the above constructed real brain FC matrices (or observed networks), we explored the generation of simulated networks based on wiring rules under different rule models. The generative network model was generated using simple wiring rules that calculated the probability of connection formation by balancing connection cost and the potential value of forming connections. Connections were probabilistically formed, and the relative probability of connecting nodes i and j was determined by a specific Eq. 1 that utilized 13 non-geometric rules to generate an energy landscape, taking into account both the Euclidean distance and power-law between nodes. The probabilistic matrix formed based on wiring rules is continuously updated over time. Starting from a sparse binary seed network, connections were gradually added until the total number of connections reaches the target value. Each connection addition considered the possibility of connecting unconnected nodes. Topological parameters were calculated using functions adapted from the Brain Connectivity Toolbox (https://sites.google.com/site/bctnet/) and previous research findings by [39].

The generative network probability was calculated as follows:

$$P_{ij} \propto \left(D_{i,j}\right)^{\eta}\left(K_{i,j}\right)^{\gamma} \tag{1}$$

where $D_{i,j}$ denotes the Euclidean distance between nodes i and j, i.e., the "cost of forming a connection", and $K_{i,j}$ denotes a specific relationship between the nodes, reflecting the value of connection formation, i.e., the "attractiveness" of forming a connection, which can be chosen from any non-geometric growth rule model used to build social and economic networks. $D_{i,j}$ is parameterized by a scalar η, which is negatively correlated with the distance between nodes, reflecting the probability that the cost of the distance between nodes affects the probability of connection formation. $K_{i,j}$ is parameterized by a scalar γ, and γ is positive. In short, the generative network grows according to the wiring equation matching rule, and connection formation between nodes prioritizes neighbouring nodes that are similarly connected and spatially proximate.

In order to find the optimal η and γ in the wiring equation to determine the appropriate probability of forming a connection between nodes, we defined the energy function (Eq. 2) to measure the level of difference between the synthetic network and the observed network, and determined the optimal parameters η and γ for each model to make the generative network closest to the observed network by minimizing E, in which the definition of KS was based on the Kolmogorov-Smirnov statistics comparing the four graph-theoretic metrics of the generated and observed networks. KS_k, KS_c, KS_b, and KS_e represented the statistics for degree, the clustering coefficient, the betweenness centrality, and the edge length distribution, respectively.

$$E = \max\left(KS_k, KS_c, KS_b, KS_e\right) \tag{2}$$

These four graph-theoretic metrics in the energy equation were good candidates for assessing the scalability of simulated networks according to previous studies [10], [11], [14], [15],

[16], [31], [39], [40], [41], in addition to being key statistical properties of network metrics and relevant to many neurological disorders [8], [9]. Their calculation formulas are as follows:

1) Degree: The degree of a node is the number of edges connected to that node. The higher the degree of a node, the more closely it is connected to other nodes. High degree nodes play a important role in the network and is more likely to influence other nodes [42]. Degree can be calculated by the following formula:

$$k_i = \sum_j A_{ij} \tag{3}$$

where A_{ij} is the FC matrix, of which the corresponding elements equal to 1 if there is a connection between nodes i and j, and 0 otherwise.

2) Clustering Coefficient: The clustering coefficient is a metric that be used to measure the degree of closeness between nodes in a network. It describes the density of connections between a node and its neighbouring nodes, indicating the probability of closed triangles forming between the adjacent nodes of a node [43]. It helps to understand the connection patterns between nodes in a network, revealing the community structure of the network and the intimacy between nodes. The formula of clustering coefficient is as follows:

$$C_i = \frac{2 * e_i}{k_i * (k_i - 1)} \tag{4}$$

where e_i is the number of edges that exist between neighbours of node i, and k_i is the degree of node i.

3) Betweenness Centrality: Betweenness centrality is a metric used to measure the extent to which a node plays an important intermediary role in a network [44]. Betweenness centrality measures the extent to which a node acts as a bridge or intermediary in a network, i.e., the node's importance in connecting other nodes in a network. Specifically, betweenness centrality is measured by counting the number of times a node acts as an intermediary node in all shortest paths [43], [44]. The formula of betweenness centrality is as follows:

$$B_i = \sum_{s \neq i \neq t} \frac{\sigma_i}{\sigma} \tag{5}$$

where σ_{st} is the total number of shortest paths from node s to node t and $\sigma_{st}(i)$ is the number of shortest paths through node i.

4) Edge Length Distribution: Edge length distribution is a statistical feature that can describe the distribution of edge lengths in a network. It reveals the distance between nodes in the network, connection patterns and network structure. The formula of edge length distribution is as follows:

$$P(d) = \frac{N(d)}{M} \tag{6}$$

where $N(d)$ is the number of edges of length d and M is the total number of edges in the graph.

Degree, clustering coefficients, median centrality, and edge length distributions can well characterize the geometric connectivity of the brain. Degree reflects the number of neurons or brain regions that are directly connected to other nodes, and nodes with a high number of heights (hub neurons or brain regions) may be responsible for integrating multiple sources of information and rapidly propagating signals through the network [42], e.g., "rich club" regions in the cortex are often characterized by a high number of heights [45]. Clustering coefficients are used to measure the degree of interconnectivity between neighbors of nodes, reflecting local modularity, with high clustering coefficients indicating dense connectivity (functional modules) within local brain regions [43], and in addition, the brain often exhibits "small-world" characteristics (high clustering as well as short pathways) to balance local processing with global integration [46]. Betweenness centrality is often used as a measure of a node's ability to act as a "bridge" between different groups, reflecting its mediating role in the global information flow [43], [44]. High median nodes may coordinate the activities of different brain regions to support complex cognitive tasks, but such nodes are vulnerable to pathological attacks (e.g., abnormalities in the salience network in schizophrenia), resulting in less efficient whole-brain communication [47]. Edge length distributions are used to define the physical or functional length distribution of connected edges in a network to observe connectivity costs and efficiencies - short edges (localized connections) conserve energy and support fast local communication, and long edges (connected across hemispheres or brain regions) facilitate global integration. Psychiatric disorders (e.g., schizophrenia) may exhibit a reduction in long connections [48], leading to functional separation; in neurodegenerative diseases, edge length distributions may reorganize, affecting network dynamics [49].

Simulations based on Eqs. 1, 2 with the approximations evaluated in previous study [39] were determined for each generative rule in a predefined parameter space of 2,500 combinations of uniform intervals ($-7 \leq \eta \leq 7$, $-7 \leq \gamma \leq 7$, with a step size of 0.28 for each interval) to determine the minimum E ranges and to estimate their relative effectiveness in generating reasonable networks based on the energy landscape maps. Subsequently, approximately 50,000-60,000 simulations were performed in a finer range of minimum energy consumption for the proximity algorithm (the range of intervals for each type of PSA at different sparsities is shown in Table. I) for all subsequent analyses. This is because the proximity algorithm yields the lowest-energy network that most closely approximates the connectivity of the real brain in the economic model. The analysis pipeline of this study is shown in Fig. 1.

D. Coefficient of Variation and Node Distribution of Cost for the Decomposition of the Wiring Equation

To determine the variability of the network generated over time, we decomposed the wiring probability ($P_{i,j}$) into two components for independent analysis: distance cost $(D_{i,j})^{\eta}$, parameterized value $(K_{i,j})^{\gamma}$ [35]. The wiring equation parameters (η and γ) for the best-simulated network of each subject were obtained through the aforementioned method. Regarding distance cost, since the static Euclidean space distance matrix was unique and deterministic, the distance

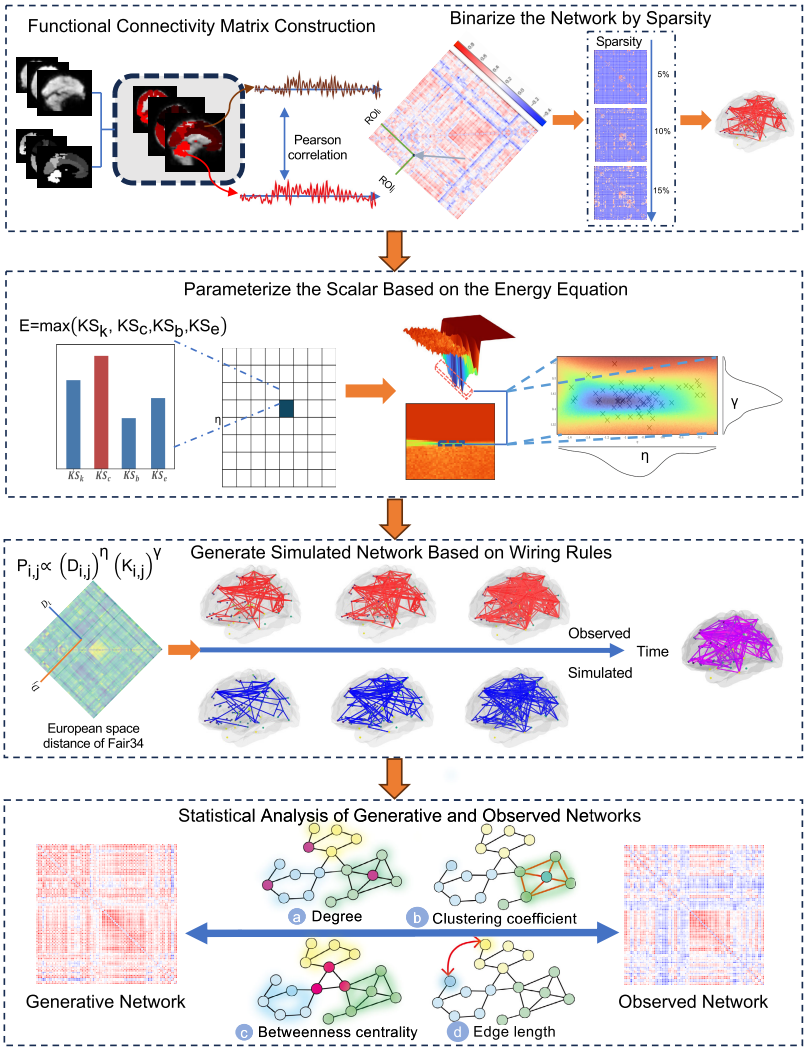

Fig. 1. The basic workflow of this investigation. **(1)** Preprocessing of the data from the dataset, including temporal layer correction, head movement correction, normalisation to a 3-mm EPI space, removal of linear drift from the signals, regression of covariates including white matter signals, cerebrospinal fluid signals, and head movement signals using the Frission −24 parametric strategy, and the use of bandwidths ranging from 0.01-0.1 Hz filtering. Brain FC matrices were constructed using Fair34 brain templates. **(2)** The initial weight matrix was binarized using different sparsities (5%, 10%, 15%) to construct a binary network. **(3)** Among the 13 wiring rules, selected the "homogeneous matching rule" with low energy consumption according to the energy equation, and run it further in the low-energy fine window. **(4)** Generated the simulated network by iteratively updating the wiring equations over time. **(5)** Statistically analyzed the graph-theoretic metrics of the observed and generated networks, comparing correlations and significant differences.

TABLE I
FINER RANGE OF MINIMUM ENERGY CONSUMPTION PARAMETERS IN NEIGHBOURHOOD ALGORITHMS FOR DIFFERENT TYPES OF PSA AT VARIOUS SPARSITIES

Sparsity	PSA Type	η	γ	Number of Simulation
5%	PSA	-2.1-1.75	0.1-0.65	60500
	None	-2.1-1.75	0.1-0.65	60500
	Healthy	-2.1-1.75	0.1-0.65	60500
10%	PSA	-2.6-2	0.35-0.65	55200
	None	-2.4-2	0.35-0.65	52800
	Healthy	-2.4-2.1	0.35-0.65	54000
15%	PSA	-2.7-2.3	0.1-0.65	55000
	None	-2.7-2.3	0.1-0.65	55000
	Healthy	-3-3.15	0.1-0.65	56320

cost for each subject was determined by the η value. For the time-varying solutions of parameterized value and wiring probability, we first computed the edges present in the network generation model at each time point, calculating their mean (μ) and standard deviation (σ) [39]. Subsequently, we determined the coefficient of variation (CV) using Eq. 7. To explore the variability of brain regions, we further summed the matrix to ascertain the changes in the node elements.

$$CV = \frac{\sigma}{\mu} \tag{7}$$

where CV stands for coefficient of variation, σ is the standard deviation, μ is the mean value.

E. Statistical Analysis

This study employed univariate linear regression analysis to evaluate the fitting effects of multiple indicators between simulated networks and real observed networks. Specifically, a p-value less than 0.05 for the regression coefficient was considered statistically significant. Additionally, the coefficient

of determination (R^2) was calculated to quantify the proportion of variation in the dependent variable that could be explained by the independent variables. To further compare the differences in energy E, η values, and γ values among patients with PSA, patients with ordinary strokes, and healthy individuals, a one-way ANOVA was conducted. Post-hoc multiple comparisons were performed using the most stringent Bonferroni correction, with a confidence level set at 95%.

III. Results

A. Results of Parameter Selection for Generative Network Models

According to the wiring rules of Eq. 1, functionally connected simulation networks were generated, where the model choice was determined by the energy equation. We initially defined the parameter ranges for η and γ ($-7 \leq \eta \leq 7$, $-7 \leq \gamma \leq 7$) and observed the generated energy landscape maps. The results and analysis process are shown in Fig. 2(A) and (B). In all samples of PSA patients, ordinary stroke patients and healthy individuals, we found that the generation networks based on homogeneity (matching and neighbours) models exhibit a more concentrated and lower energy distribution compared to other generative rules. Although the degree-based average rule (D-Avg) had the lowest average energy, its low energy distribution was uneven, making it difficult to further identify low-energy bands for fine-tuning simulations [39]. This suggests that the economic cost generated by the homogeneity model in conjunction with geometric distance can produce optimal simulated networks.

Based on the generated energy landscape, further optimization of the economical model parameters was conducted to match the topological profiles of brain networks (Fig. 2(C)), with relevant parameters shown in Table. I. Within the selected narrow low-energy band range, simulations were performed between 50,000 to 60,000 times, resulting in finely tuned networks with lower energy compared to previous analyses.

We further analyzed the relevance of four graph-theoretic metrics used for energy E optimization between observed and simulated networks. It was observed from Fig. S1 (see Supplementary materials) that degree ($R = 0.41$, $p = 0.015$), betweenness centrality ($R = 0.51$, $p = 0.0017$), and edge lengths ($R = 0.76$, $p =$ 1.59e-07) exhibited significant positive correlations between observed and generated networks. However, clustering coefficients ($R = 0.22$, $p = 0.21$) did not show a significant correlation. That is, spatial embedding of these network properties appeared to reflect the observed network, and although not specified during growth, simple homogeneity rules gave rise to many of the observed brain network properties according to previous study [39].

To demonstrate whether these spatial patterns of network properties solely arise from the generated model, node efficiency was introduced as an external evaluation metric. It was observed that there remained a significant positive correlation (shown in Supplementary Fig. S2) between observed and generated networks ($R = 0.34$, $p = 0.04$), confirming the similarity in node properties between generated and observed networks. In addition, component differences were analyzed for the simulated network (right panel) and the observation network (left panel). They were consistent in binary networks with 10% sparsity.

To eliminate subjective factors in the binarization of sparse matrices, we incorporated binarized matrices with sparsity levels of 5% and 15% as comparisons. We found that as the sparsity increased, the correlation and significance of the nodes' degree, betweenness centrality, and clustering coefficient exhibited a notable decline. The edge length showed the highest significance at a sparsity level of 10%, while the other metrics demonstrated varying degrees of decline compared to the binarized network results generated at 10% sparsity. This suggested that simulating network generation based on wiring rules using the binarized matrix at 10% sparsity yields optimal simulation results. The results of the comparison between the generative network and the actual functional network at different sparsities are given in detail in Table S1 of the Supplementary Material.

B. Differences in Generative Network Model Parameters for Stroke and PSA

Further, when comparing the parameters η and γ of the generated networks, we found significant differences between PSA patients and general stroke patients, the results are shown in Fig. 3. Specifically, the absolute value of η was larger for PSA patients compared to general stroke patients ($p = 0.0174$), indicating that aphasic patients incurred higher economic costs in forming connections with distant nodes. Furthermore, PSA patients exhibited the highest γ, suggesting a lower tendency for connections between nodes compared to healthy controls, with significant differences observed ($p = 0.0304$).

These findings were consistent in brain networks with a sparsity of 15%. In simulated networks at 15% sparsity, both η and γ for PSA patients remained significantly higher compared to the other two groups. Specifically, the difference in η between PSA patients and general stroke patients increased significantly ($p < 0.0001$) compared to networks with 10% sparsity. However, the significant difference in γ between PSA patients and healthy controls observed in the 10% sparsity networks disappeared ($p = 0.2559$) in the 15% sparsity networks.

In summary, it was shown that PSA patients differed significantly from ordinary stroke patients and healthy controls in terms of the economic cost of brain network connectivity and the propensity to connect, with PSA patients having significantly higher η values, especially in networks with a sparsity of 15%, whereas the γ difference tended to disappear at higher sparsities.

C. Variability of Parameter Combinations Leading to Changes in Connection Generation Trajectories

From Eq. 1, it is easily found that small parameter differences can lead to different generative networks. To further investigate how such differences arise with the formation and development of network connections, we quantified the network connection formation trajectory by decomposing Eq. 1 in terms of distance cost $(D_{i,j})^{\eta}$, parameterized value $(K_{i,j})^{\gamma}$, and wiring probability $(P_{i,j})$ at each time point for each

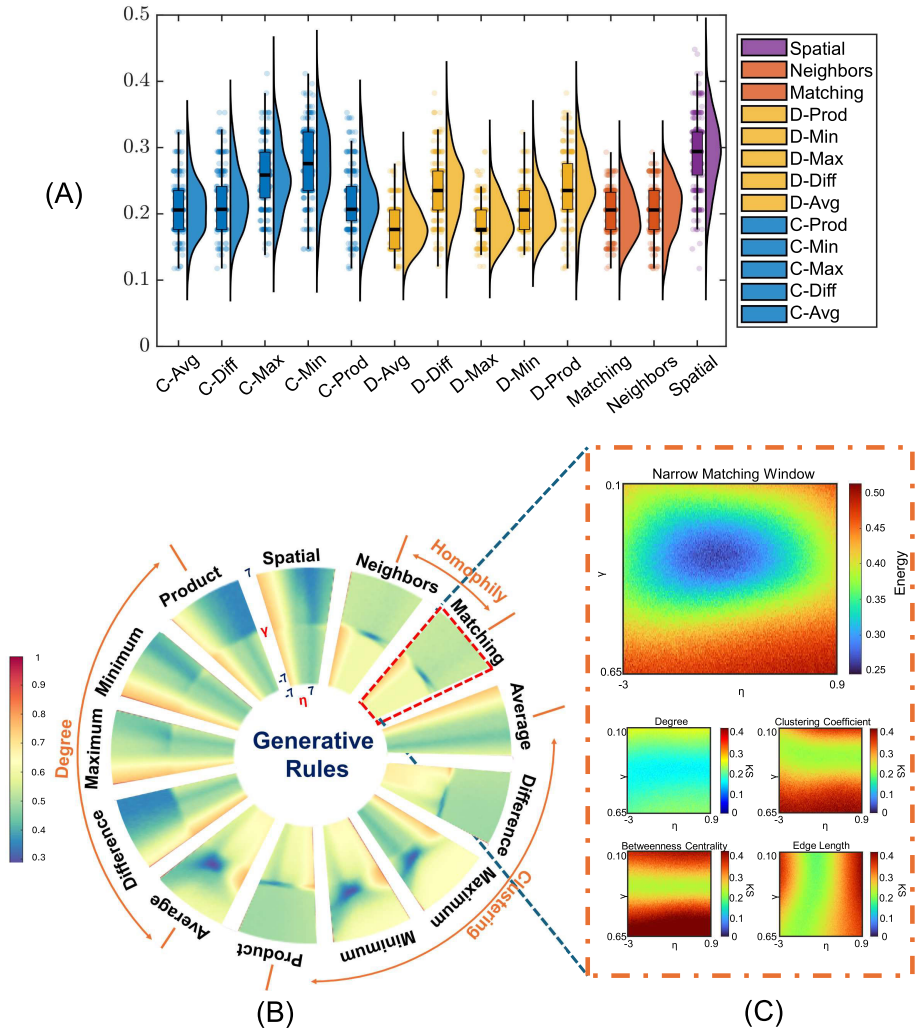

Fig. 2. Visualization of the average energy E difference of samples under different generation rules. **(A)** A violin diagram of energy statistics from 13 generation rules for optimal performance simulation. The central black dot in the box diagram represents the median of the data, and the box length is used to measure the dispersion of the data. The box plot is covered by the kernel density map, and the larger the area of the graph in a certain area, the greater the probability of distribution near a certain value. The scatter points in the violin represent each individual data. **(B)** The homogeneity-based methods calculate the shared neighborhood measure between nodes using matching and neighbor algorithms. Spatial methods entirely ignore γ and rely solely on spatial relationships for network assessment. Clustering-based methods compute the aggregate measure between two nodes using their clustering coefficients. Degree-based methods determine the aggregate measure between two nodes based on their degrees. In the energy landscape diagram of 13 different models with a total of 2,500 parameter combinations, the darker the blue colour, the lower the energy consumption of forming connections. **(C)** Among the 13 wiring rules, selected the "homogeneous matching rule" with low energy consumption according to the energy equation, and run it further in the low-energy narrow window. The global landscape map with 50,000-60000 parameter combinations was determined under the "matching" rule, and the relationship between energy and KS statistics of four local indexes involved in energy function calculation (node degree, cluster coefficient, betweenness centrality and edge length) under different parameter combinations was determined.

subject under the optimal simulation parameter combinations (η and γ) to observe the differences of network connection formation trajectories in PSA, healthy, and normal stroke. Observing the variability exhibited at the level of the cortex and their connections between PSA, healthy, and normal stroke subjects, and thus to determine which aspects of network formation differ the most, and to examine their differences at the group level.

For all subjects in each group, we calculated the coefficient of variation (CV) for their distance cost $(D_{i,j})^{\eta}$, parameterized value $(K_{i,j})^{\gamma}$, and wiring probability $(P_{i,j})$ to compare the variability of subject-specific coefficients during the iterative process of generating simulated networks (See Fig. 4). Fig. 4a exhibits the CV of the three items decomposed in the wiring equation, and it is clear that the CV of the wiring probability is the largest, while the CV of the parameterized value is much larger than the CV of the distance cost. Fig. 4b further collapses the subjects based on network nodes on the basis of Fig. 4a, showing the spatial distribution of parameterized value and distance cost of the brain, and a clear difference can be seen in the three groups. In addition, as shown in Fig. 4b, the spatial patterns of distance costs and parameterized values were not random but showed some regularity. For patients with PSA, the parameterized values were relatively evenly

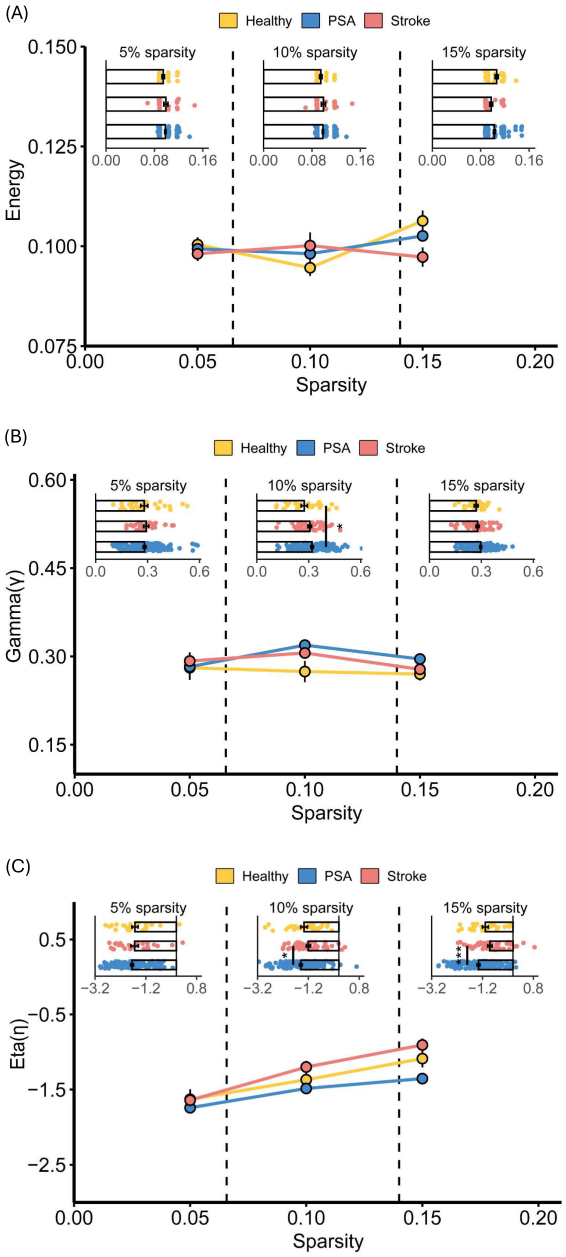

Fig. 3. In generative binary networks with 5%, 10%, and 15% sparsity levels, one-way ANOVA was used to compare the intergroup significance differences in energy E **(A)**, gamma η **(B)**, and eta γ **(C)** among patients with PSA, general stroke patients, and healthy controls.

distributed across the nodes, whereas in healthy individuals and ordinary stroke patients, the parameterized values were mainly concentrated in the medial cortex, especially in the anterior part of the thalamus and the middle part of the cingulate cortex. Notably, the distribution of distance costs was similar in patients with PSA and healthy individuals, with high distance costs mainly concentrated in the lateral cortex, whereas ordinary stroke patients showed the opposite distribution pattern.

In order to further investigate the relationship between the distance cost of nodes for PSA and healthy subjects compared to that of ordinary stroke subjects, we conducted a linear analysis of the nodes, with results illustrated in Fig. 5. The distance cost of nodes for PSA and healthy subjects showed a significant negative correlation with the distance cost of nodes for ordinary stroke patients ($R^2 = 0.86$ and $R^2 = 0.94$, respectively).

IV. Discussion

We explored a wiring generation modelling approach that balances the cost of forming connections with the potential value of those connections. The equation iteratively renegotiated its costs and values across parameter combinations, thereby minimising energy costs to optimise connection probabilities [50]. Importantly, connection probabilities changed dynamically over time, reflecting the interactive nature of real brain functional connectivity [27], [34], [35], [39]. This dynamic change was simulated and remodelled using constraint equations to quantify how stroke and PSA remodel and alter brain connectivity. In the wiring generation model, every time a node formed a new connection, it dynamically changed the topological properties of its neighbours, which affected the attractiveness of the remaining nodes to form subsequent connections until the number of generated connections matched the number of observed networks [51]. Therefore, we further observed the dynamic characteristics of the generated network based on the static analysis of the network, and in the analysis of the unwrapping of the wiring equation, we found that there were significant differences in the parameterized value and distance cost of the nodes at the time of the formation of the probabilistic connections between PSA, common stroke and healthy subjects. The following summary will further discuss the results we obtained:

A. Selection of Homogeneity Rules for the Wiring Equation

We found that the simulated networks generated based on homogeneity rules consumed less energy compared to those generated by other rules except for Average and Max Degree-based methods. Although D-Max and D-Avg perform better in terms of energy consumption compared to Neighbor and Matching methods, degree-based methods optimized the wiring design mainly by considering the degree of a node. However, this approach focuses mainly on local information and tends to ignore the importance of global optimization. This limitation explained the inconsistency in the performance of the five models based on degree; compared to the two models based on homogeneity, the degree-based approach appeared to be weaker in terms of stability and was more likely to fall into a locally optimal solution. Given that the primary objective of brain network operation was to achieve optimal computational capacity within limited biological resources [34], [35], we could infer that the simulated networks generated by homogeneity rules are closer to the whole-brain network. Although different regions within the whole-brain network exhibited anatomical and functional differences, their interconnectivity and modes of information transmission might adhere to certain common rules or principles [39]. This was akin to the dynamic coordination and synchronization among different regions of

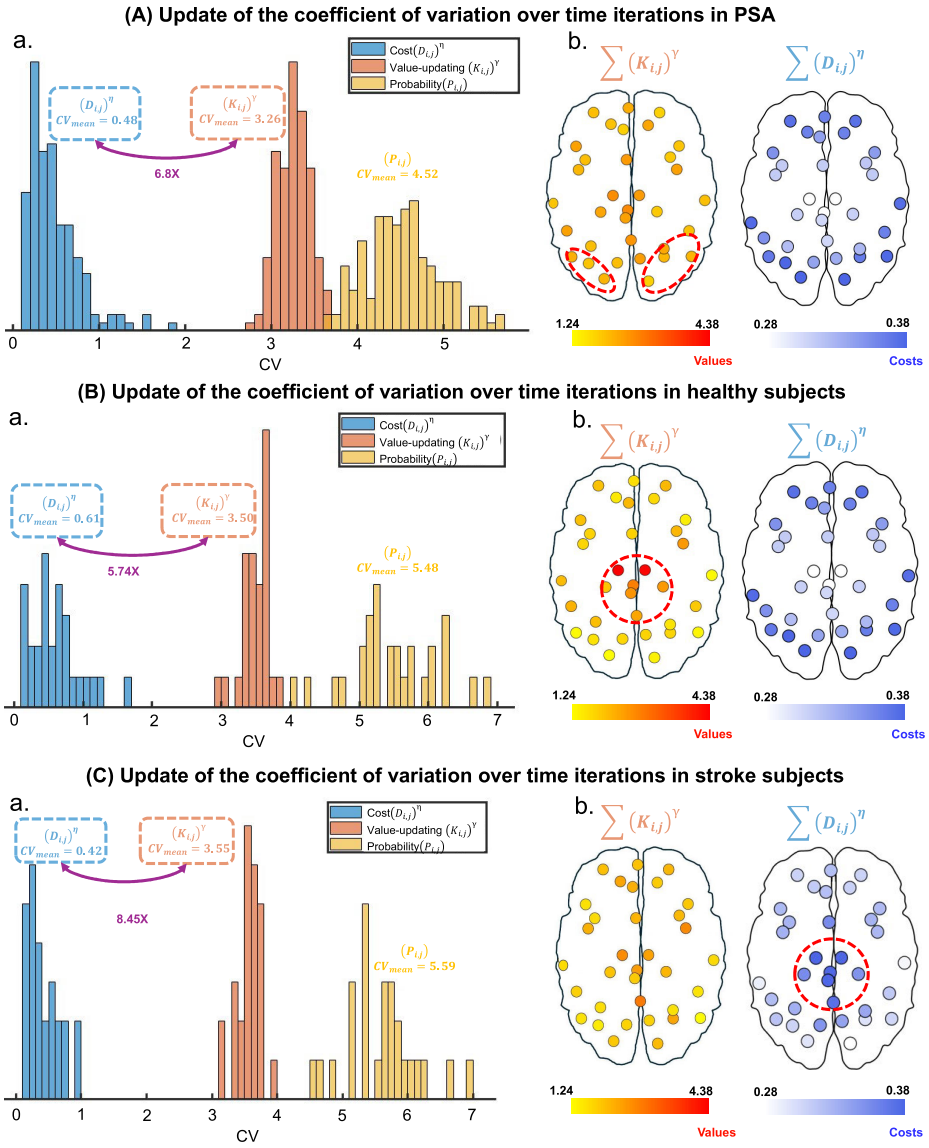

Fig. 4. The wiring probability $(P_{i,j})$ was divided into two components for independent analysis: distance cost $(D_{i,j})^{\eta}$ was uniquely determined by the η value for each subject, and parameterized cost $(K_{i,j})^{\gamma}$, on the other hand, was dynamically updated with the matching rule. **(A)**, **(B)**, and **(C)** correspond to the coefficient of variation (CV) analysis of the iterative parameters updated over time for PSA, healthy, and normal stroke patients, respectively, where **a** denotes the histogram of the CV of the distance cost $(D_{i,j})^{\eta}$, parameterized cost $(K_{i,j})^{\gamma}$, and wiring probability $(P_{i,j})$ for the group, and **b** denotes the distribution of $(D_{i,j})^{\eta}$ and $(K_{i,j})^{\gamma}$ in the brain of samples within the group.

the whole-brain network. The generation rule model based on homogeneity might aim to capture specific features of such dynamic network models, such as the pathways and integration methods of information transmission, which could incur lower informational costs and thus be more biologically plausible [35], [39].

B. Effect of the Choice of Sparsities on the Simulation Results

In the results, we were surprised to find that simulated generative brain networks according to wiring rules were significantly influenced by sparsity. In sparse networks, the limited number of connections between nodes results in a low probability of mutual connections among neighbouring nodes, making it difficult to form strong community structures [52]. Consequently, the lack of effective local structural clustering features in sparse networks hinders the clustering coefficient from accurately reflecting the complex interactions and cluster structures that may exist in real networks [53], [54]. Furthermore, sparse networks tend to have irregular topological structures, lacking clear structural and modular characteristics, which diminishes the effectiveness of the fitting model in capturing these features [55]. This explains why simulated networks generated from low-sparsity binary networks were unable to effectively fit the real observed brain networks in terms of clustering coefficients and local node efficiency.

In contrast, in dense networks, there is often a higher probability of connections among neighbouring nodes, which may lead to an increased clustering coefficient. However, when the network approaches a fully connected network, the

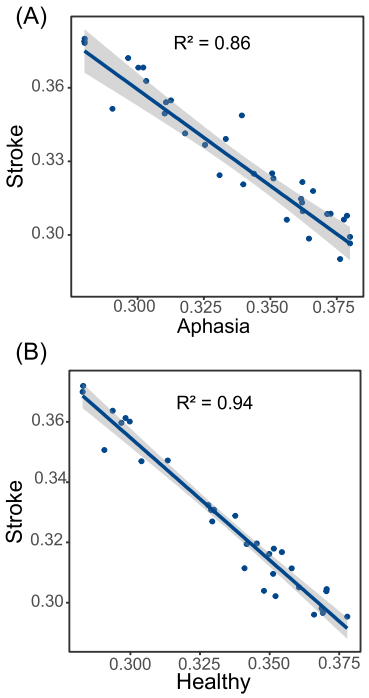

Fig. 5. Linear correlation of distance cost $(D_{i,j})^{\eta}$ between different groups. **(A)** indicates a linear correlation of $(D_{i,j})^{\eta}$ for regular stroke subjects with PSA patients, and **(B)** indicates a linear correlation of $(D_{i,j})^{\eta}$ for regular stroke subjects with healthy subjects.

clustering coefficient may tend toward 1, making it difficult for the model to accurately capture and distinguish subtle variations in high clustering coefficients, resulting in poor fitting performance [55]. Additionally, in dense networks, the shortest paths between nodes are relatively short, and many nodes have fewer opportunities to act as bridges within these paths, which may lead to a concentrated distribution of betweenness centrality [53], [54]. Certain nodes may exhibit excessively high betweenness centrality, while others may have significantly low values. The calculation of betweenness centrality in dense networks may be influenced by edge density, thereby affecting the fitting results. The dense connectivity of the networks makes it more challenging to reflect the differences between the simulated networks and the actual networks, as the real networks may exhibit uneven connection patterns or unique structural features, making this discrepancy more pronounced in dense networks [56].

C. Higher η Indicates More Long-Range FCs in PSA Patients

We also noted that previous studies have consistently demonstrated significant differences in the topological features of PSA compared to healthy populations, including longer characteristic path lengths, lower clustering coefficients, and reduced local node efficiency [15], [35]. This shift towards a more random network topology can be simulated through generative models that reduce the distance penalty parameter (η), thereby increasing the probability of long-range connections. This explains why the absolute value of η is greater in PSA and shows significant differences when compared to typical stroke patients. This finding resonates with some prior neuroimaging results, suggesting that the brain networks of PSA may possess a greater number of long-range connections than those in normal brain networks [15], [35]. This provides a valuable reference for future research utilizing network formation model parameters to summarize and understand other neurological disorders.

D. Variability of Distance Costs and Parameterized Values Shows Different Network-Generated Trajectories for PSA and Stroke Patients

It is easy to see from Fig. 4a that while the effect of distance cost on the probability of connection generation exhibits a certain degree of variability (CV = 0.48, 0.61 and 0.42), the parameterized values change dynamically over time as the simulated brain network is continuously updated and iterated, leading to larger coefficients of variation (CV = 3.26, 3.50 and 3.55). This leads to significant individual differences in wiring probabilities, indicating inter-individual differences in brain organization. Among the three groups of subjects, healthy subjects had the largest mean coefficient of variation for distance costs and the smallest difference from the mean coefficient of variation for parameterized values, which may be attributed to the relative functional integrity of the brain and individual differences [39]. The average coefficient of variation of distance cost was smaller in normal stroke patients and PSA patients due to the occurrence of acute brain injury resulting in the loss of FC between site-specific nodes.

In Fig. 4b, parameterized values are increased in the lateral parietal lobe, lateral cerebellum, and inferior cerebellum in patients with PSA compared with healthy and normal stroke patients. Distance cost node distributions are similar between PSA and healthy individuals, with higher distance costs in the limbic nodes of the brain, but the distribution is in the opposite direction from that of normal stroke patients (see Fig. 5 for the linear relationship). More notably, the parameterized values are lower in the thalamus of PSA and normal stroke patients compared with healthy individuals, but the distance cost is higher in the thalamus of normal stroke patients. This may be due to the fact that the thalamus is the relay station for most sensory information (closely linked to language-related regions such as Broca and Wernicke [57]), which receives sensory signals from the body other than smell and further transmits them to the cerebral cortex for processing [58], which is consistent with the finding that damage to the thalamus may be associated with PSA [57], [59], [60], [61]. In addition, higher parameterized values are found in the occipital lobes of the right and left sides of brain with the inferior cerebellum in PSA patients compared to normal stroke and healthy subjects, which is consistent with the finding that there may be functionally relevant restoration of or residual speech functioning in aphasic patients with enhanced activity in the vicinity of the cerebellum following brain damage [62], [63].

E. Comparison With Previous Studies of PSA With FC and Brain Networks

Previous research has consistently highlighted substantial differences in the topological characteristics of PSA compared to healthy populations, including longer characteristic path

lengths, lower clustering coefficients, and reduced local node efficiency [15], [35], alongside a reduction in small-worldness and normalized clustering coefficients [16]. Additionally, brain network strength and overall efficiency have been linked to the treatment outcomes in PSA patients [24]. While graph theory-based metrics have proven useful in identifying biomarkers by contrasting healthy and PSA patients, they offer limited understanding of the underlying mechanisms governing network function, growth, and evolution [27]. Therefore, we introduced the network generative model, which serves as a versatile framework for generating synthetic networks based on parameterized wiring rules [30], [31]. By integrating multiple rules to simulate the formation of functional brain networks, this study is expected to reveal specific brain network evolution mechanisms associated with aphasia and explain the PSA-related network features found by previous studies. For example, the reduction of the distance penalty parameter (η) in PSA could increasing the probability of long-range connections, and this explains why the brain networks of PSA may possess a greater number of long-range connections than those in normal brain networks [15], [35].

F. Limitations and Future Directions

Although our results demonstrate that these models are statistically robust, a good fit of the model does not necessarily prove that the brain network optimizes model parameters by calculating minimal energy consumption through specific metrics. Moreover, for some local metrics, the generated simulated networks do not fit well, indicating that future work needs to further explore the impact of different node counts in brain templates and the selection of binary sparsity on the generation of simulated networks. In addition, this computational framework still has limitations. Our generative model is restricted to producing simple binary networks while neglecting the complex weighted structural information inherent within the networks [39], [64]. Developing methods to enable network connections to change in a more gradual manner is next step in generative modeling, which presents opportunities for future improvements to the model to achieve a more accurate fit with observed networks.

V. Conclusion

The human functional brain network exhibits a complex topological structure, with this complexity arising from the connections and interactions between different regions of the brain. When constructing spatial geometric functional connections, this process can be viewed as a trade-off between geometric distance and the propensity for connections between nodes. The consistency of the constructed mathematical models of simulated brain networks with observed metrics of real brain networks indicates the effectiveness of these models in capturing the essence of brain FC. For patients with PSA, the differences in the parameters of their brain network models compared to those of typical stroke patients and healthy individuals may reflect the unique characteristics of language processing and cognitive function in PSA. Further analysis of the parameter changes in the process of dynamic formation of probabilistic connections based on the wiring rule model showed that the parameterized value and distance cost of PSA in the thalamus, occipital lobe and cerebellum regions were significantly different from those in healthy people and ordinary stroke patients. These differences can provide a mathematical explanation for the distinctive topological structure observed in PSA, offering deeper insights into the process of functional reorganization in the brain under this pathological condition.

References

[1] V. L. Feigin et al., "Global, regional, and national burden of stroke and its risk factors, 1990–2019: A systematic analysis for the global burden of disease study 2019," *Lancet Neurol.*, vol. 20, no. 10, pp. 795–820, 2021.

[2] J. Bernhardt et al., "Agreed definitions and a shared vision for new standards in stroke recovery research: The stroke recovery and rehabilitation roundtable taskforce," *Int. J. Stroke*, vol. 12, no. 5, pp. 444–450, Jul. 2017.

[3] M. Varkanitsa and S. Kiran, "Insights gained over 60 years on factors shaping post-stroke aphasia recovery: A commentary on vignolo (1964)," *Cortex*, vol. 170, pp. 90–100, Jan. 2024.

[4] S. M. Sheppard and R. Sebastian, "Diagnosing and managing post-stroke aphasia," *Expert Rev. Neurotherapeutics*, vol. 21, no. 2, pp. 221–234, Feb. 2021.

[5] M. Rubinov and O. Sporns, "Complex network measures of brain connectivity: Uses and interpretations," *NeuroImage*, vol. 52, no. 3, pp. 1059–1069, Sep. 2010.

[6] S. Whitfield-Gabrieli and A. Nieto-Castanon, "Conn: A functional connectivity toolbox for correlated and anticorrelated brain networks," *Brain Connectivity*, vol. 2, no. 3, pp. 125–141, Jun. 2012.

[7] J. Wang, X. Wang, M. Xia, X. Liao, A. Evans, and Y. He, "GRETNA: A graph theoretical network analysis toolbox for imaging connectomics," *Frontiers Hum. Neurosci.*, vol. 9, p. 386, Jun. 2015.

[8] H.-C. Baggio et al., "Functional brain networks and cognitive deficits in Parkinson's disease," *Hum. Brain Mapping*, vol. 35, no. 9, pp. 4620–4634, Sep. 2014.

[9] J. Kim et al., "Abnormal intrinsic brain functional network dynamics in Parkinson's disease," *Brain*, vol. 140, no. 11, pp. 2955–2967, Nov. 2017.

[10] E. L. Dennis and P. M. Thompson, "Functional brain connectivity using fMRI in aging and Alzheimer's disease," *Neuropsychol. Rev.*, vol. 24, no. 1, pp. 49–62, Mar. 2014.

[11] J. DelEtoile and H. Adeli, "Graph theory and brain connectivity in Alzheimer's disease," *Neuroscientist*, vol. 23, no. 6, pp. 616–626, 2017.

[12] S. N. Miri Ashtiani et al., "Altered topological properties of brain networks in the early MS patients revealed by cognitive task-related fMRI and graph theory," *Biomed. Signal Process. Control*, vol. 40, pp. 385–395, Feb. 2018.

[13] F. V. Farahani, W. Karwowski, and N. R. Lighthall, "Application of graph theory for identifying connectivity patterns in human brain networks: A systematic review," *Frontiers Neurosci.*, vol. 13, p. 585, Jun. 2019.

[14] F. Agosta et al., "Disrupted brain connectome in semantic variant of primary progressive aphasia," *Neurobiol. Aging*, vol. 35, no. 11, pp. 2646–2655, Nov. 2014.

[15] Y. Tao, B. Ficek, B. Rapp, and K. Tsapkini, "Different patterns of functional network reorganization across the variants of primary progressive aphasia: A graph-theoretic analysis," *Neurobiol. Aging*, vol. 96, pp. 184–196, Dec. 2020.

[16] X. Chen et al., "Disrupted brain connectivity networks in aphasia revealed by resting-state fMRI," *Frontiers Aging Neurosci.*, vol. 13, Oct. 2021, Art. no. 666301.

[17] D. S. Bassett and E. Bullmore, "Small-world brain networks," *Neuroscientist*, vol. 12, no. 6, pp. 512–523, Dec. 2006.

[18] L. K. Gallos, M. Sigman, and H. A. Makse, "The conundrum of functional brain networks: Small-world efficiency or fractal modularity," *Frontiers Physiol.*, vol. 3, p. 123, Jan. 2012.

[19] Zamora-López, "Cortical hubs form a module for multisensory integration on top of the hierarchy of cortical networks," *Frontiers Neuroinform.*, vol. 4, p. 613, Mar. 2010.

[20] M. Guye, G. Bettus, F. Bartolomei, and P. J. Cozzone, "Graph theoretical analysis of structural and functional connectivity MRI in normal and pathological brain networks," *Magn. Reson. Mater. Phys., Biol. Med.*, vol. 23, nos. 5–6, pp. 409–421, Dec. 2010.

[21] E. Bullmore and O. Sporns, "Complex brain networks: Graph theoretical analysis of structural and functional systems," *Nature Rev. Neurosci.*, vol. 10, no. 3, pp. 186–198, Mar. 2009.

[22] O. Sporns, "Contributions and challenges for network models in cognitive neuroscience," *Nature Neurosci.*, vol. 17, no. 5, pp. 652–660, May 2014.

[23] M. P. van den Heuvel and O. Sporns, "Rich-club organization of the human connectome," *J. Neurosci.*, vol. 31, no. 44, pp. 15775–15786, Nov. 2011.

[24] J. P. Johnson, E. L. Meier, Y. Pan, and S. Kiran, "Pre-treatment graph measures of a functional semantic network are associated with naming therapy outcomes in chronic aphasia," *Brain Lang.*, vol. 207, Aug. 2020, Art. no. 104809.

[25] O. Sporns, "Network attributes for segregation and integration in the human brain," *Current Opinion Neurobiol.*, vol. 23, no. 2, pp. 162–171, Apr. 2013.

[26] E. Bullmore and O. Sporns, "The economy of brain network organization," *Nature Rev. Neurosci.*, vol. 13, no. 5, pp. 336–349, May 2012.

[27] R. F. Betzel and D. S. Bassett, "Generative models for network neuroscience: Prospects and promise," *J. Roy. Soc. Interface*, vol. 14, no. 136, Nov. 2017, Art. no. 20170623.

[28] R. M. Lazar and D. Antoniello, "Variability in recovery from aphasia," *Current Neurol. Neurosci. Rep.*, vol. 8, no. 6, pp. 497–502, Nov. 2008.

[29] D. C. Tippett, "Update in aphasia research," *Current Neurol. Neurosci. Rep.*, vol. 15, no. 8, pp. 1–8, Aug. 2015.

[30] P. Erdős and A. Rényi, "On the evolution of random graphs," *Publ. Math. Inst. Hung. Acad. Sci.*, vol. 5, no. 1, pp. 17–60, 1960.

[31] D. J. Watts and S. H. Strogatz, "Collective dynamics of 'small-world' networks," *Nature*, vol. 393, no. 6684, pp. 440–442, 1998.

[32] M. Rubinov, "Constraints and spandrels of interareal connectomes," *Nature Commun.*, vol. 7, no. 1, p. 13812, Dec. 2016.

[33] A. C. Murphy and D. S. Bassett, "A network neuroscience of neurofeedback for clinical translation," *Current Opinion Biomed. Eng.*, vol. 1, pp. 63–70, Mar. 2017.

[34] R. F. Betzel et al., "Generative models of the human connectome," *NeuroImage*, vol. 124, pp. 1054–1064, Jan. 2016.

[35] P. E. Vértes, A. F. Alexander-Bloch, N. Gogtay, J. N. Giedd, J. L. Rapoport, and E. T. Bullmore, "Simple models of human brain functional networks," *Proc. Nat. Acad. Sci. USA*, vol. 109, no. 15, pp. 5868–5873, Apr. 2012.

[36] M. Gibson et al., "The aphasia recovery cohort, an open-source chronic stroke repository," *Sci. Data*, vol. 11, no. 1, p. 981, Sep. 2024.

[37] C. N. Wahlheim, A. P. Christensen, Z. M. Reagh, and B. S. Cassidy, "Intrinsic functional connectivity in the default mode network predicts mnemonic discrimination: A connectome-based modeling approach," *Hippocampus*, vol. 32, no. 1, pp. 21–37, Jan. 2022.

[38] D. A. Fair et al., "Functional brain networks develop from a 'local to distributed' organization," *PLoS Comput. Biol.*, vol. 5, no. 5, 2009, Art. no. e1000381.

[39] D. Akarca et al., "A generative network model of neurodevelopmental diversity in structural brain organization," *Nature Commun.*, vol. 12, no. 1, p. 4216, Jul. 2021.

[40] A.-L. Barabási and R. Albert, "Emergence of scaling in random networks," *Science*, vol. 286, no. 5439, pp. 509–512, Oct. 1999.

[41] R. Albert and A. Barabási, "Statistical mechanics of complex networks," *Rev. Modern Phys.*, vol. 74, no. 1, pp. 47–97, 2002.

[42] J. L. Gross, J. Yellen, and M. Anderson, *Graph Theory and Its Applications*. London, U.K.: Chapman & Hall, 2018.

[43] B. C. M. van Wijk, C. J. Stam, and A. Daffertshofer, "Comparing brain networks of different size and connectivity density using graph theory," *PLoS ONE*, vol. 5, no. 10, Oct. 2010, Art. no. e13701.

[44] Y. Iturria-Medina, R. C. Sotero, E. J. Canales-Rodríguez, Y. Alemán-Gómez, and L. Melie-García, "Studying the human brain anatomical network via diffusion-weighted MRI and graph theory," *NeuroImage*, vol. 40, no. 3, pp. 1064–1076, Apr. 2008.

[45] N. A. Crossley et al., "The hubs of the human connectome are generally implicated in the anatomy of brain disorders," *Brain*, vol. 137, no. 8, pp. 2382–2395, Aug. 2014.

[46] O. Sporns and R. F. Betzel, "Modular brain networks," *Annu. Rev. Psychol.*, vol. 67, no. 1, pp. 613–640, Jan. 2016.

[47] A. Manoliu et al., "Aberrant dependence of default mode/central executive network interactions on anterior insular salience network activity in schizophrenia," *Schizophrenia Bull.*, vol. 40, no. 2, pp. 428–437, Mar. 2014.

[48] L. Rutter et al., "Graph theoretical analysis of resting magnetoencephalographic functional connectivity networks," *Frontiers Comput. Neurosci.*, vol. 7, p. 93, Jul. 2013.

[49] S. Fornari, A. Schäfer, M. Jucker, A. Goriely, and E. Kuhl, "Prion-like spreading of Alzheimer's disease within the brain's connectome," *J. Roy. Soc. Interface*, vol. 16, no. 159, Oct. 2019, Art. no. 20190356.

[50] S. Nandy, *A Theoretical Framework for Generative Modeling of Human Functional Brain Networks*. Richardson, TX, USA: Univ. Texas at Dallas, 2018.

[51] R. F. Betzel et al., "The modular organization of human anatomical brain networks: Accounting for the cost of wiring," *Netw. Neurosci.*, vol. 1, no. 1, pp. 42–68, Feb. 2017.

[52] H. Eavani, T. D. Satterthwaite, R. Filipovych, R. E. Gur, R. C. Gur, and C. Davatzikos, "Identifying sparse connectivity patterns in the brain using resting-state fMRI," *NeuroImage*, vol. 105, pp. 286–299, Jan. 2015.

[53] B. Cassidy, C. Rae, and V. Solo, "Brain activity: Connectivity, sparsity, and mutual information," *IEEE Trans. Med. Imag.*, vol. 34, no. 4, pp. 846–860, Apr. 2015.

[54] Z. Boukouvalas, Y. Levin-Schwartz, V. D. Calhoun, and T. Adalı, "Sparsity and independence: Balancing two objectives in optimization for source separation with application to fMRI analysis," *J. Franklin Inst.*, vol. 355, no. 4, pp. 1873–1887, Mar. 2018.

[55] B. Ge et al., "Signal sampling for efficient sparse representation of resting state FMRI data," *Brain Imag. Behav.*, vol. 10, no. 4, pp. 1206–1222, Dec. 2016.

[56] S. Bandyopadhyay, S. Peddi, M. Sarma, and D. Samanta, "Decoding autism: Uncovering patterns in brain connectivity through sparsity analysis with rs-fMRI data," *J. Neurosci. Methods*, vol. 405, May 2024, Art. no. 110100.

[57] S. Ozturk, F. Ege, and H. Ekmekci, "Language disorders due to posterior system Strokes–An ignored dysfunction," *Noro Psikiyatri Arsivi*, vol. 51, no. 4, pp. 313–317, Dec. 2014.

[58] J. M. Shine, L. D. Lewis, D. D. Garrett, and K. Hwang, "The impact of the human thalamus on brain-wide information processing," *Nature Rev. Neurosci.*, vol. 24, no. 7, pp. 416–430, Jul. 2023.

[59] L. De Witte, J. Verhoeven, S. Engelborghs, P. P. De Deyn, and P. Mariën, "Crossed aphasia and visuo-spatial neglect following a right thalamic stroke: A case study and review of the literature," *Behavioural Neurol.*, vol. 19, no. 4, pp. 177–194, Jan. 2008.

[60] M. Fritsch, I. Rangus, and C. H. Nolte, "Thalamic aphasia: A review," *Current Neurol. Neurosci. Rep.*, vol. 22, no. 12, pp. 855–865, Dec. 2022.

[61] S. Maeshima and A. Osawa, "Thalamic lesions and aphasia or neglect," *Current Neurol. Neurosci. Rep.*, vol. 18, no. 7, pp. 1–6, Jul. 2018.

[62] L. T. Connor, T. D. Braby, A. Z. Snyder, C. Lewis, V. Blasi, and M. Corbetta, "Cerebellar activity switches hemispheres with cerebral recovery in aphasia," *Neuropsychologia*, vol. 44, no. 2, pp. 171–177, Jan. 2006.

[63] M. E. Vasilopoulou and L. C. Triarhou, "Neurobiological and pathophysiological concepts of christfried jakob (1866–1956) on language and aphasia: An english translation of two communications [1910,1932] and a modern perspective," *J. Chem. Neuroanatomy*, vol. 133, Nov. 2023, Art. no. 102341.

[64] O. Tymofiyeva, C. P. Hess, D. Xu, and A. J. Barkovich, "Structural MRI connectome in development: Challenges of the changing brain," *Brit. J. Radiol.*, vol. 87, no. 1039, Jul. 2014, Art. no. 20140086.